ACS APPLIED MATERIALS & INTERFACES

Research Article

www.acsami.org

A Gel–Polymer Sn–C/$LiMn_{0.5}Fe_{0.5}PO_4$ Battery Using a Fluorine-Free Salt

Daniele Di Lecce,[†] Chiara Fasciani,[‡] Bruno Scrosati,[‡] and Jusef Hassoun*[,†,§]

[†]Dipartimento di Chimica, Sapienza Università di Roma, P.le Aldo Moro 5, 00185 Rome, Italy

[‡]Istituto Italiano di Tecnologia, 00161 Rome, Italy

[§]Dipartimento di Scienze Chimiche e Farmaceutiche, Università di Ferrara, Via Fossato di Mortara 17, 44121 Ferrara, Italy

Supporting Information

ABSTRACT: Safety and environmental issues, because of the contemporary use of common liquid electrolytes, fluorinated salts, and $LiCoO_2$-based cathodes in commercial Li-ion batteries, might be efficiently mitigated by employing alternative gel–polymer battery configurations and new electrode materials. Herein we study a lithium-ion polymer cell formed by combining a $LiMn_{0.5}Fe_{0.5}PO_4$ olivine cathode, prepared by simple solvothermal pathway, a nanostructured Sn–C anode, and a LiBOB-containing PVdF-based gel electrolyte. The polymer electrolyte, here analyzed in terms of electrochemical stability by impedance spectroscopy (EIS) and voltammetry, reveals full compatibility for cell application. The LiBOB electrolyte salt and the electrochemically delithiaded $Mn_{0.5}Fe_{0.5}PO_4$ have a higher thermal stability compared to conventional $LiPF_6$ and $Li_{0.5}CoO_2$, as confirmed by thermogravimetric analysis (TGA) and by galvanostatic cycling at high temperature. $LiMn_{0.5}Fe_{0.5}PO_4$ and Sn–C, showing in lithium half-cell a capacity of about 120 and 350 mAh g^{-1}, respectively, within the gelled electrolyte configuration are combined in a full Li-ion polymer battery delivering a stable capacity of about 110 mAh g^{-1}, with working voltage ranging from 2.8 to 3.6 V.

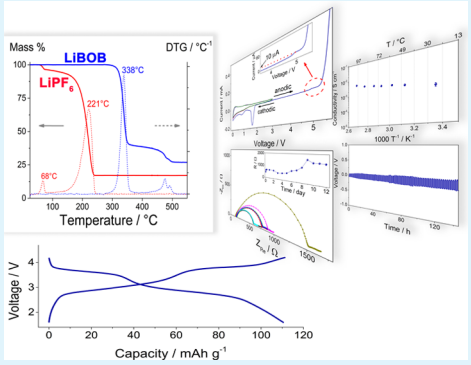

KEYWORDS: *gel–polymer electrolyte, LiBOB, LiMn0.5Fe0.5PO4, Sn–C, solvothermal synthesis, Li-ion battery*

INTRODUCTION

Hazards related to the use of fluorinated salts, e.g., $LiPF_6$, in conventional alkyl carbonate liquid solvents as well as environmental and safety issues associated to cobalt-based electrodes, including the common $LiCoO_2$ layered cathode, represent severe concerns hindering a fully safe employment of the commercial Li-ion batteries (LIBs).[1,2] Indeed, $LiPF_6$ salt is characterized by a thermal stability limited to moderate temperatures,[3] and may react with possible H_2O traces to form HF by hydrolysis, thus leading to electrode deterioration, cell damage, and final capacity fading.[4,5] Furthermore, $Li_{1-x}CoO_2$ phases ($x \leq 0.5$) may decompose and release oxygen at high temperatures, with consequent thermal runaway risks in case of short-circuit of lithium-ion cells employing volatile and flammable carbonate-based electrolytes.[1] Therefore, new electrode and electrolyte components are required to effectively overcome the current LIBs safety issues.[6]

In this respect the advantages of all-solid configurations have triggered deep efforts on the development of polymer electrolytes having high room-temperature ionic conductivity and satisfactory transference number. Dry polymer electrolytes, such as poly(ethylene oxide) (PEO)-based ones, do not incorporate liquid components and show low conductivity at room temperature. On the other hand, electrolyte solutions may be efficiently confined in polymer matrixes of remarkable affinity with the alkyl carbonates, thus forming a gel polymer electrolyte (GPE) having hybrid features of both liquid and solid systems. The GPE has high room-temperature ionic conductivity because of the trapped liquid electrolyte, and is characterized by increased mechanical and chemical stability and low electrolyte leakage due to the polymeric network. Among the polymer hosts proposed for GPE applications, such as poly(ethylene oxide) (PEO), poly(acrylonitrile) (PAN), poly(methyl methacrylate) (PMMA), poly(vinylidene fluoride) (PVdF), poly(vinylidene fluoride-hexafluoro propylene) (PVdF-HFP), PVdF-based matrixes have been extensively studied for lithium-ion battery applications, because of their high chemical stability and affinity with the liquid component.[7,8]

The safety content of the gel polymer battery may be further improved by replacing the conventional $LiPF_6$ electrolyte salt by fluorine-free salts, having higher thermal stability, thus matching important requirements of power-grid and automotive markets.[9] Lithium bis(oxalato)borate (LiBOB) has shown suitable properties, both as additive and as electrolyte salt in fluorine-free solutions for application in lithium batteries.[10−14]

Received: June 11, 2015
Accepted: September 8, 2015
Published: September 8, 2015

DOI: 10.1021/acsami.5b05179
ACS Appl. Mater. Interfaces 2015, 7, 21198−21207

Indeed, LiBOB shows a remarkable thermal stability, compared to $LiPF_6$, and favorable solid electrolyte interphase (SEI), in particular at the carbonaceous anode surface, preventing the undesired cointercalation of solvent molecules during cell operation.[5,15−17] It has been demonstrated that electrolytes using a mixed LiBOB/$LiPF_6$ salt in carbonate-based solution may actually improve the capacity retention of LIBs at the higher temperature levels (e.g., 50 °C).[18]

However, the LiBOB salt is characterized by a lower solubility in carbonate solvent mixtures, leading to a limited ionic conductivity in respect to $LiPF_6$-containing solutions.[19] In addition, the common $Li_{1-x}CoO_2$ cathode shows a poor stability in LiBOB-based electrolytes, in particular in its charged state and at the higher temperature levels. Instead, $LiFePO_4$ olivine cathode reveals remarkable high-temperature stability in LiBOB-alkyl carbonates solutions.[20] A literature study proposed a solution formed by dissolving 0.7 M of LiBOB in EC:PC:DMC (1:1:3) as suitable electrolyte for lithium-ion batteries, combining satisfactory salt concentration, with consequent high ionic conductivity, and low viscosity because of the high amount of DMC.[21] This liquid electrolyte has been employed in a promising Sn−C/$LiFePO_4$ lithium-ion battery in a previous paper.[22] In a recent report,[23] Aravindan et al. described the favorable features of alloying anodes in full cell configurations. In particular, Sn−C composites show stable cycling behavior in LIBs using conventional as well as advanced cathode materials ($LiCoO_2$, $LiFePO_4$, $LiNi_{0.5}M_{1.5}O_4$, $LiFe_{0.1}Co_{0.9}PO_4$). Sn−C electrode shows a capacity of about 500 mAh g^{-1}, i.e., a higher value in respect to common electrodes such as graphite (370 mAh g^{-1}) and lithium titanium oxide (170 mAh g^{-1}), as well as enhanced cycling life in a wide temperature range. Further improvement of the gel polymer battery, in terms of energy density, may be achieved by using $LiMn_{1-x}Fe_xPO_4$ olivine cathode instead of $LiFePO_4$, due to an increase of the cell working voltage due to the higher potential of Mn^{3+}/Mn^{2+} redox reaction (4.1 V vs. Li^+/Li) in respect to Fe^{3+}/Fe^{2+} one (3.45 V vs. Li^+/Li).[24−37]

Accordingly, we report herein a gel polymer Li-ion cell formed by combining a $LiMn_{0.5}Fe_{0.5}PO_4$ cathode, a nanocomposite Sn−C anode,[38] and a 0.7 M LiBOB in EC:PC:DMC 1:1:3-PVdF gel polymer electrolyte (GPE). The battery herein studied differs from the ones previously reported employing Sn−C anode by the expected enhanced energy and safety content, deriving from the contemporary use of a stable olivine cathode and LiBOB-containing GPE. Indeed, the olivine electrode, including not only Fe but also Mn in its formulation, allows higher working voltage in respect to bare $LiFePO_4$, whereas the gelled electrolyte based on LiBOB salt is suitable for application at the higher temperatures without ongoing decomposition or fluorinated compounds release. Several literature papers have mainly focused on the improvement of the $LiMn_{0.5}Fe_{0.5}PO_4$ olivine cathode performances in lithium half-cell employing conventional liquid electrolyte. Therefore, we believe that the Li-ion cell here reported may also provide useful contribution to $LiMn_{0.5}Fe_{0.5}PO_4$ study in an alternative full-cell configuration.

The $LiMn_{0.5}Fe_{0.5}PO_4$ cathode is prepared by a simple solvothermal method and characterized. The electrochemical features of the GPE are investigated in terms of temperature-dependent ionic conductivity, electrochemical stability, lithium interface, as well as by galvanostatic cycling tests in half-cells using the Sn−C alloying electrode and the $LiMn_{0.5}Fe_{0.5}PO_4$ olivine cathode. Thermogravimetric analyses (TGA) confirmed the higher thermal stability of the LiBOB salt, the GPE, and the electrochemically delithiated $Mn_{0.5}Fe_{0.5}PO_4$ cathode in respect to conventional $LiPF_6$, conventional alkyl carbonate liquid electrolyte, and $Li_{1-x}CoO_2$, respectively. Galvanostatic cycling tests at high temperature are used to investigate the effect of LiBOB salt on the cell performances. In conclusion, the full Sn−C/GPE/$LiMn_{0.5}Fe_{0.5}PO_4$ polymer Li-ion battery, revealing promising features in terms of electrochemical behavior and thermal stability of the components, is proposed as an example of suitable energy storage system characterized by expected high safety and low cost.

EXPERIMENTAL SECTION

The $LiMn_{0.5}Fe_{0.5}PO_4$ olivine material was obtained by a solvothermal method optimized in our laboratories.[39] Two water solutions, one containing lithium hydroxide monohydrate ($LiOH·H_2O$) and another containing lithium dihydrogen phosphate (LiH_2PO_4), $MnSO_4·H_2O$, $FeSO_4·H_2O$, and sucrose were added to ethylene glycol (EG) under vigorous stirring (final ratio EG:H_2O 2:1 v/v). The molar ratios of LiH_2PO_4, $MnSO_4·H_2O$, $FeSO_4·7H_2O$, $LiOH·H_2O$, and sucrose were 1:0.5:0.5:1.75:0.03. The obtained suspension was sealed into a Teflon-lined autoclave and heated in oven at 180 °C for 20 h. The reaction product was filtered, washed with water and ethanol, and dried in oven at 70 °C. $LiMn_{0.5}Fe_{0.5}PO_4$ was carbon-coated by pyrolysis technique. The $LiMn_{0.5}Fe_{0.5}PO_4$ sample was suspended in a sucrose/water solution (molar ratio $LiMn_{0.5}Fe_{0.5}PO_4$/sucrose = 80:20% w/w) and heated at 60 °C in a rotary evaporator in order to totally remove water and thus precipitate a homogeneous sucrose layer on the particles surface. The powder above obtained was heated at 700 °C for 3 h under an Ar atmosphere to produce a black $LiMn_{0.5}Fe_{0.5}PO_4$/C composite. Thermogravimetric analysis (TGA; SDTA 851 Mettler-Toledo), performed in a 60 mL min^{-1} air flow at a scanning rate of 10 °C min^{-1} from 25 to 900 °C, confirmed a final carbon content of about 5 wt % (data not reported). The XRD experiment was carried out by using a Rigaku Xray Ultima$^+$ diffractometer equipped with a Cu Kα source and a graphite monocromator for the diffracted beam.

The gel polymer electrolyte (GPE) was prepared by swelling a dry poly(vinylidene fluoride)-based (Solef Solvay, PVdF 6020) membrane in a solution of 0.7 M lithium bis(oxalate)borate (LiBOB, Chemetall) in a 1:1:3 weight ratio ethylene carbonate/propylene carbonate/dimethyl carbonate (EC/PC/DMC, Merck) solvent. The PVdF-based membrane was prepared under air, according to a procedure described in a previous work,[40] and then swollen in an Ar-filled glovebox. The swelling was carried out by immersing the dry membrane in the electrolyte solution for 12 h in order to trap the electrolyte within the PVdF matrix. This preparation procedure allowed a final electrolyte/PVdF weight ratio of about 80:20.[40] The ionic conductivity of the gel polymer electrolyte was measured by impedance spectroscopy on blocking-electrode coin-cell, by using a multichannel potentiostat/galvanostat analyzer VersaSTAT MC, Princeton Applied Research (PAR) (10 mV amplitude signal, frequency range 100 kHz−100 Hz). The properties of the Li/GPE interface at open circuit voltage (OCV) condition were evaluated by impedance spectroscopy analyses carried out on Li/Li symmetrical cells, by using a multichannel potentiostat/galvanostat VSP Bio-Logic (10 mV amplitude signal, frequency range 500 kHz−10 mHz). The polarization associated with the lithium dissolution/plating at the Li/GPE interface was studied by galvanostatically cycling (current = 100 μA cm^{-2}, step time = 1 h) a Li/Li symmetrical cell. The electrochemical stability window of the GPE membrane was determined by linear sweep voltammetry (LSV) and by cyclic voltammetry (CV) through a Bio-Logic VMP potentiostat. The measures were performed at a scan rate of 0.1 mV s^{-1}, by using two-electrode cells with Super P Carbon-coated (Timcal) Al or Cu foils as the working electrode (weight ratio Super P:PVdF binder = 80:20%) and lithium foil as the counter electrode.

The GPE was studied in combination with the $LiMn_{0.5}Fe_{0.5}PO_4$ olivine cathode and a Sn−C nanocomposite anode synthesized in our laboratories (the synthesis of Sn−C is already described in a previous

DOI: 10.1021/acsami.5b05179
ACS Appl. Mater. Interfaces 2015, 7, 21198−21207

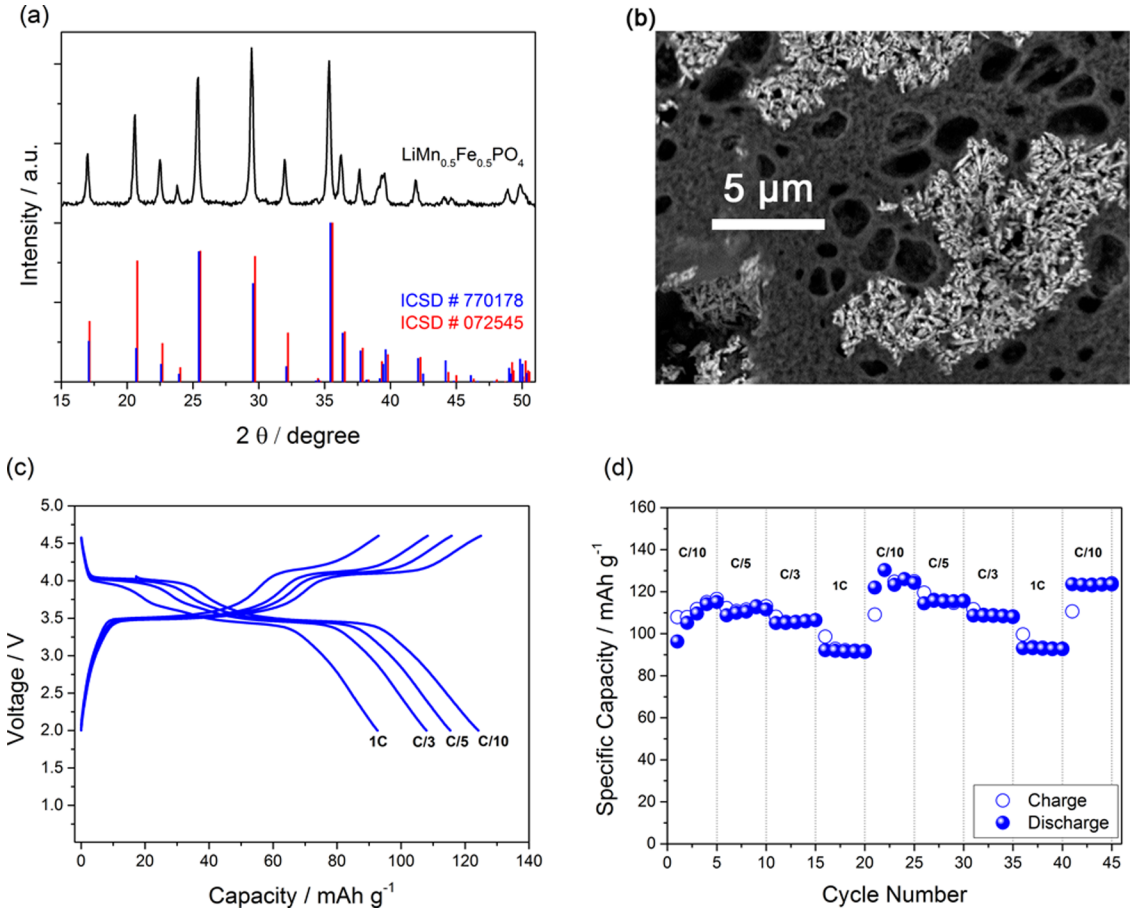

Figure 1. (a) X-ray diffraction (XRD) patterns of the $LiMn_{0.5}Fe_{0.5}PO_4$ powder, $LiFePO_4$ (ICSD # 072545), and $LiMnPO_4$ (ICSD # 770178) references. (b) Scanning electron micrograph (SEM) of $LiMn_{0.5}Fe_{0.5}PO_4$. (c) Galvanostatic voltage profiles and (d) corresponding cycling behavior of $LiMn_{0.5}Fe_{0.5}PO_4$ electrode used in lithium half-cell with LP30 electrolyte at increasing current rates, i.e., 0.1*C*, 0.2*C*, 0.33*C*, and 1*C*, respectively (1*C* = 170 mA g^{-1}). Voltage limits 2.0−4.6 V. Room temperature (25 °C).

paper).[41] The $LiMn_{0.5}Fe_{0.5}PO_4$ electrodes were prepared by mixing active material powder (AM), a PVdF-HFP (Kynar Flex 2801) binder, and Super P Carbon (weight ratio 80:10:10%) in tetrahydrofuran (THF, Sigma-Aldrich). The resulting slurry was deposited on carbon cloth-based current collectors and cast, with a final mass loading of about 3 mg cm^{-2} following a vacuum drying step at 110 °C overnight. The $LiMn_{0.5}Fe_{0.5}PO_4$ electrodes were tested in lithium half-cell with standard electrolyte solution (1 M $LiPF_6$ EC/DMC 1:1 w/w, LP30, BASF, battery grade) by galvanostatic cycling within 2−4.6 V voltage range at various current rates (0.1*C*, 0.2*C*, 0.33*C*, 1*C*; 1*C* = 170 mA g^{-1}). The Sn−C electrodes were prepared by mixing the AM, a PVdF binder (6020, Solef Solvay), and Super P Carbon (weight ratio 80:10:10%) in N-methyl pyrrolidone (NMP, Sigma-Aldrich). The resulting slurry was deposited on cupper foils and cast, with a final mass loading of about 2 mg cm^{-2} following a vacuum drying step at 110 °C overnight. Lithium polymer half-cells were assembled by coupling the electrode under test with a GPE and a lithium foil counter electrode. The Li/GPE/$LiMn_{0.5}Fe_{0.5}PO_4$ half-cell was tested within 2−4.5 V voltage range at 0.1C rate. The Li/GPE/Sn−C half-cell was tested within 0.01−2 V voltage range at 50 mA g^{-1} (about C/8).

The full lithium-ion polymer batteries were assembled by stacking $LiMn_{0.5}Fe_{0.5}PO_4$ cathode, GPE, and Sn−C anode. Prior to half- and full-cells assembling, the Sn−C electrode was partially prelithiated by galvanostatic cycling in lithium cell with a 1 M $LiPF_6$ EC/DMC 1:1 w/w (LP30, BASF, battery grade) electrolyte solution, soaked on a Whatman glass math separator, at 100 mA g^{-1} within 0.01−2.0 V voltage range. After prelithiation, the anode was washed with DMC before half- and full-cell assembling, in order to remove LP30 traces from electrode surface. The full cells were prepared by using an excess of cathode material to partially fit the anode capacity. The Sn−C/GPE/$LiMn_{0.5}Fe_{0.5}PO_4$ cells were cycled within the 1.6−4.2 V voltage range at 0.1C and 0.2C rates in respect to the cathode electrode (1*C* = 170 mA $g_{cathode}^{-1}$). A full Sn−C/$LiMn_{0.5}Fe_{0.5}PO_4$ cell employing standard LP30 electrolyte was also assembled, by coupling a fresh $LiMn_{0.5}Fe_{0.5}PO_4$ and a prelithiated Sn−C electrodes, and tested in order to balance the cathode/anode mass ratio (see Supporting Information). The Sn−C/$LiMn_{0.5}Fe_{0.5}PO_4$ cell employing standard LP30 electrolyte was cycled within the 1.8−4.5 V voltage range at 0.2C rate in respect to the cathode electrode (1*C* = 170 mA $g_{cathode}^{-1}$). All the cells were assembled in Ar-filled glovebox. Swagelok T-type cells (electrode diameter = 10 mm) were used for galvanostatic cycling in a Maccor 4000 series battery test system.

Galvanostatic cycling tests at 70 °C on two Li/$LiMn_{0.5}Fe_{0.5}PO_4$ coin-cells using Whatman glass math separator soaked in LP30 and 0.7 M LiBOB in EC/PC/DMC 1:1:3 w/w liquid electrolytes, respectively, were performed in order to compare the thermal stability of $LiPF_6$ and LiBOB salts in lithium cell. Thermogravimetric analysis (TGA) were carried out in order to compare the thermal stability of LiBOB salt, delithiated $Mn_{0.5}Fe_{0.5}PO_4$ electrode, and LiBOB-containing GPE with conventional $LiPF_6$ (Merck, battery grade), $Li_{1-x}CoO_2$, and Whatman glass math separator soaked in LP30, respectively. The TGA experiments were performed under a 60 mL min^{-1} N_2 flow at a heating rate of 10 °C min^{-1} from 25 °C. LiBOB salt was dried for 24 h under vacuum at 120 °C before use. Both salts were stored in Ar-filled glovebox. Delithiated $Mn_{0.5}Fe_{0.5}PO_4$ and $Li_{1-x}CoO_2$ powders were obtained by galvanostatic charge in lithium cell using LP30 electrolyte at 0.2 mA cm^2. The cells were prepared by employing cathode round

DOI: 10.1021/acsami.5b05179
ACS Appl. Mater. Interfaces 2015, 7, 21198−21207

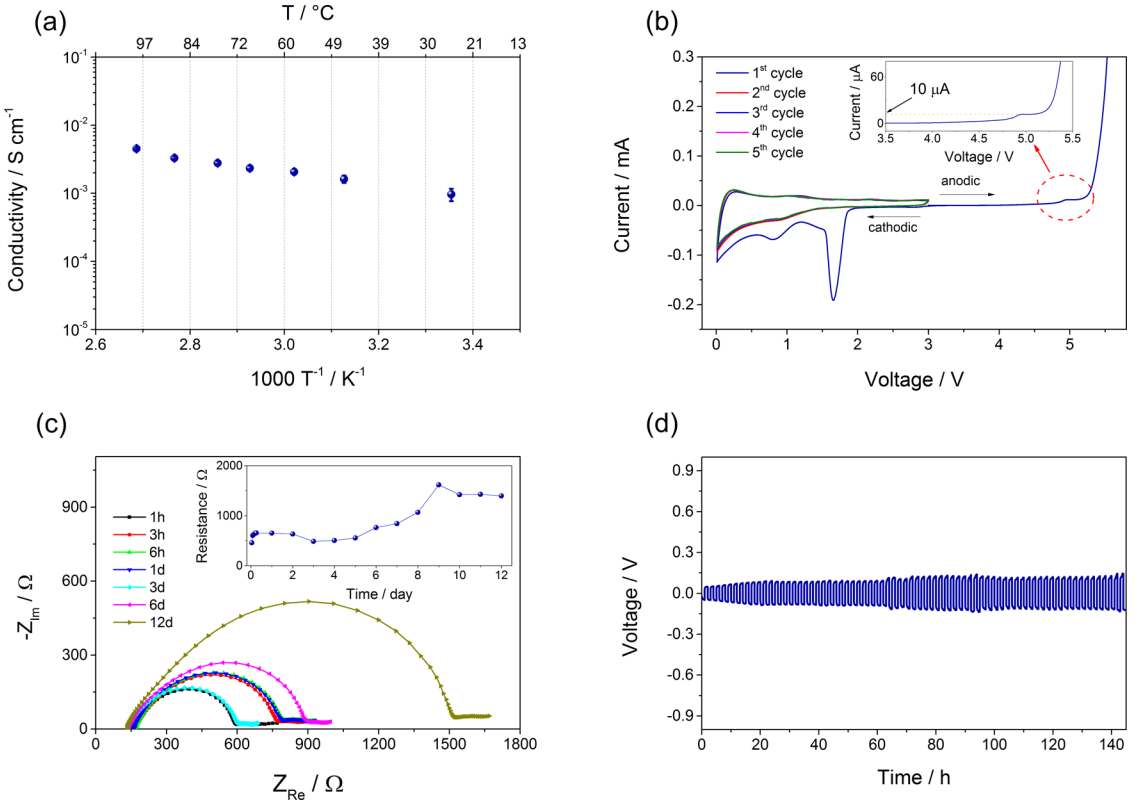

Figure 2. Electrochemical properties of the GPE. (a) Arrhenius conductivity plot determined by electrochemical impedance spectroscopy (EIS) experiments using a SS/GPE/SS coin-cell. (b) Electrochemical stability window of the GPE, as determined by linear sweep voltammetry (LSV) and cyclic voltammetry (CV) at 0.1 mV s^{-1} scan rate using Super P Carbon working electrode and lithium foil counter electrode. (c) Nyquist impedance spectroscopy plot of Li/GPE/Li symmetrical cell at OCV (10 mV amplitude signal, frequency range 500 kHz−10 mHz); in inset time dependence of interfacial resistance calculated by nonlinear least-squares (NNLS) analysis. (d) Galvanostatic lithium dissolution/plating of Li/GPE/Li symmetrical cell (current = 100 μA cm^{-2}, step time = 1 h).

pellets (1 cm diameter) of 25 mg and 40 mg for $LiCoO_2$ (SC 15, Merck) and $LiMn_{0.5}Fe_{0.5}PO_4$, respectively. After charge, the cells were disassembled in Ar-filled glovebox to recover the cathode materials for analysis. The electrodes were washed several times with DMC and dried for 15 min under vacuum.

Scanning electron microscopy (SEM) images of $LiCoO_2$, $LiMn_{0.5}Fe_{0.5}PO_4$, and corresponding charged electrode powders were taken using a Phenom-FEI instrument.

RESULTS AND DISCUSSION

Figure 1a shows the XRD pattern of the $LiMn_{0.5}Fe_{0.5}PO_4$ cathode, indexed to single olivine phase with a *Pnmb* space group, without signs of impurities. The comparison of the experimental XRD pattern with the $LiFePO_4$ (ICSD # 072545) and $LiMnPO_4$ (ICSD # 770178) reference data confirms the formation of a solid solution without aggregation of $LiFePO_4$ and $LiMnPO_4$ phases. The scanning electron micrograph (SEM) of the $LiMn_{0.5}Fe_{0.5}PO_4$ cathode, reported in Figure 1b, indicates homogeneous morphology and submicrometrical particles (maximum size below 1 μm), without signs of segregation. These morphological features are a compromise in terms of particle size, which can ensure an efficient electrochemical process by contemporary limiting the electrolyte decomposition and shortening the lithium diffusion pathways.

The cathode was preliminary tested in lithium half-cells with LP30 electrolyte by galvanostatic cycling at various current rates (see Figure 1c, d, reporting the voltage profiles and corresponding cycling behavior, respectively) as well as following a single current rate procedure, i.e., at 0.2*C* rate (see Figure S1). After few initial activation cycles, most likely due to a structural reorganization of the pristine olivine structure already observed for $LiMn_{0.5}Fe_{0.5}PO_4$,[25] the figures show a reversible discharge capacity of about 123, 115, 108, 93 mAh g^{-1} at 0.1*C*, 0.2*C*, 0.33*C*, and 1*C* rates, respectively (see Figure 1c, d), and a Coulombic efficiency approaching 100% (see Figure S1). The $LiMn_{0.5}Fe_{0.5}PO_4$ cathode reversibly exchanges lithium ions with two plateaus, centered at about 3.5 and 4.1 V, associated with the Fe^{3+}/Fe^{2+}[42] and Mn^{3+}/Mn^{2+}[24] electrochemical reactions, respectively, (see Figure 1c). In particular, the electrochemical features are comparable to those reported for others $LiMn_{0.5}Fe_{0.5}PO_4$ materials prepared by solvothermal pathway.[25,37]

Figure 2 shows the characteristics of the LiBOB-containing GPE in terms of conductivity at several temperatures (Arrhenius plot in panel a) and electrochemical stability window (panel b). Figure 2a reveals a room temperature (RT) ionic conductivity of about 1×10^{-3} S cm^{-1}, i.e., a suitable value for lithium cell operation. The ionic conductivity of the LiBOB-containing GPE is similar to that ascribed to $LiPF_6$-based GPEs[8,43] and higher than that of PEO-based systems.[44] The electrochemical stability of the GPE has been investigated both in the cathodic and in the anodic region by cyclic voltammetry (CV) and linear sweep voltammetry (LSV), respectively. For the purpose, a Super P working electrode was used in order to evaluate possible occurrence of parasitic phenomena during cell operation at the electrode/electrolyte interface (see Figure 2b). Indeed, the anodic scan reveals a

DOI: 10.1021/acsami.5b05179
ACS Appl. Mater. Interfaces 2015, 7, 21198−21207

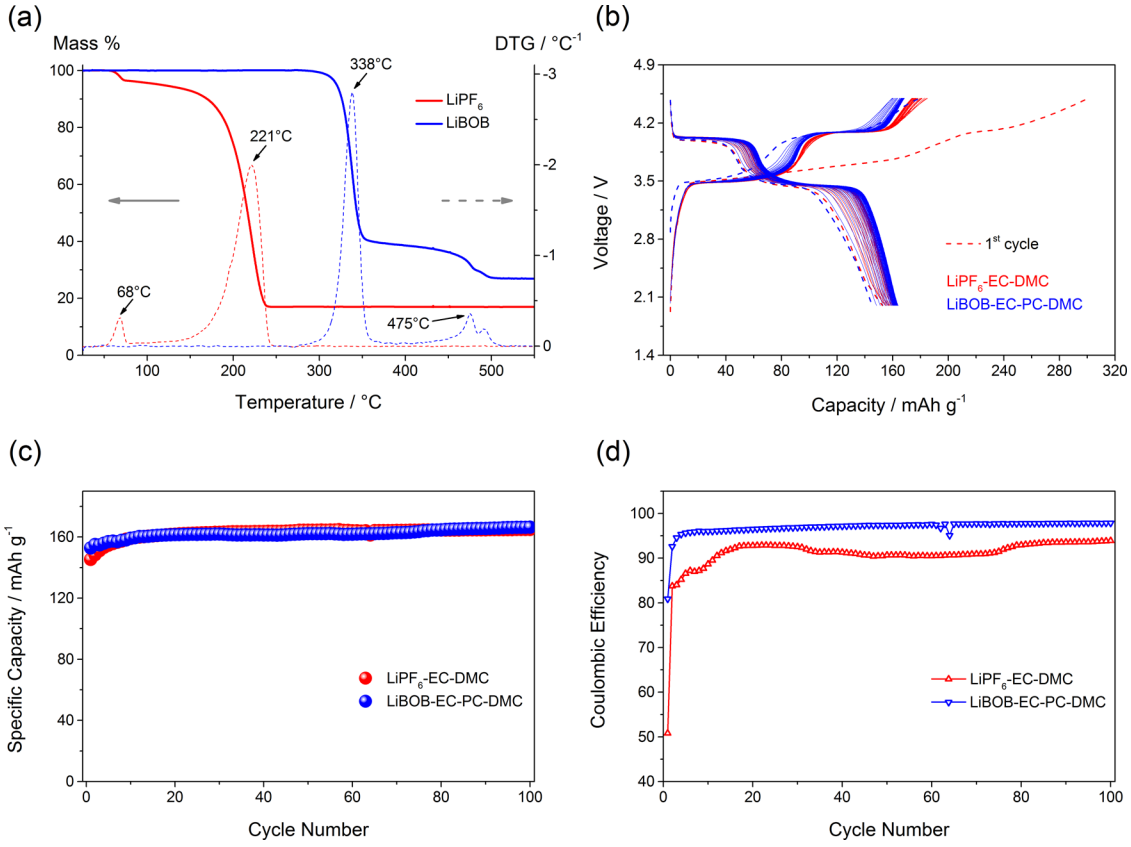

Figure 3. (a) Thermogravimetric analysis (TGA) of $LiPF_6$ (red) and LiBOB (blue) salts performed under a 60 mL min^{-1} N_2 flow at a heating rate of 10 °C min^{-1}. Mass percent on the left *y* axis (continuous line) and derivative curve (dotted line) on the right *y* axis. Galvanostatic cycling results at 70 °C in terms of (b) voltage profiles, (c) discharge capacity, and (d) Coulombic efficiency for two $Li/LiMn_{0.5}Fe_{0.5}PO_4$ half-cells using LP30 and 0.7 M LiBOB EC/PC/DMC 1:1:3 w/w liquid electrolytes, respectively. Test performed within 2−4.5 V voltage range at 1*C* rate (170 mA g^{-1}).

current onset around 4.9 V, which remains stable at 10 μA until increasing above 5.1 V because of oxidation of the electrolyte, namely a suitable high-voltage value for LIBs application.

Meanwhile, the cathodic voltammetry displays different features during the first cycle in respect to the following cycles. A narrow peak at about 1.7 V, followed by a broader peak, appears throughout the first reduction scan, while in the next cycles minor overlapped peaks suggest the presence of reversible electrochemical reactions. In previous works,[15,22,45] LiBOB has been reported to contribute, in alkyl carbonate solvents, to SEI formation on carbonaceous anodes surface through electrochemical irreversible reduction around 1.7 V, i.e., according to the onset potential observed in Figure 2b. The overlapped peaks in the following cycles can be ascribed to minor reversible lithium insertion/deinsertion within the amorphous carbon matrix at the very low potential regions.

The bottom panels of Figure 2 (Figure 2c, d) report the characteristics of the GPE interphase against lithium metal. The impedance measurement of the Li/GPE/Li symmetrical cell at open circuit voltage condition (OCV) reveals an initial interfacial resistance of about 460 Ω (see Figure 2c). During the first 4 h, the impedance time-evolution shows an interfacial resistance increasing to about 550 Ω, followed by a slight decrease and stabilization upon 6 days of storage. However, the figure shows a final resistance of about 1.5 kΩ, thus suggesting poor stability of the GPE interphase upon long storage in contact with lithium metal. Similar indication has been obtained by Li/GPE interface investigation under dynamic condition, by lithium galvanostatic dissolution/plating experiment conducted in symmetrical lithium cell (Figure 2d). This analysis shows an increase of the polarization associated with the lithium oxidation/reduction processes, which remains, however, limited to 200 mV.

In summary, the suitable membrane conductivity and its electrochemical stability, extending up 4.9 V, are expected to allow an efficient and safe operation in battery. However, the continuous growth of the Li/GPE interfacial resistance suggests the replacement of the lithium metal with a Li-ion anode as suitable solution for efficient use of a polymer full-cell configuration having improved reliability. In particular, as already mentioned, the polymer-battery configuration studied here is supposed to have enhanced chemical and thermal stability, due to the fluorine-free salt as well as the stable polyanionic framework of the olivine cathode.

The higher thermal stability of LiBOB salt, when compared to that of conventional $LiPF_6$, was confirmed by running thermogravimetric analysis (TGA) under N_2 flow. Figure 3a shows TGA results comparison, on the left *y*-axis, as well as derivative TG (DTG) curves, on the right *y*-axis, for both LiBOB and $LiPF_6$ salts (see Experimental Section). $LiPF_6$ shows a decomposition starting at about 60 °C, with a first slight weight loss of 4% (see DGT peak at 68 °C in Figure 3a) and a subsequent massive loss, i.e., of about 80% (see DGT peak at 221 °C in Figure 3a). The thermal behavior of $LiPF_6$ has been already investigated by TGA,[21,46,47] however, depending on the adopted experimental conditions, different onset decomposition temperatures have been reported. In

DOI: 10.1021/acsami.5b05179
ACS Appl. Mater. Interfaces 2015, 7, 21198−21207

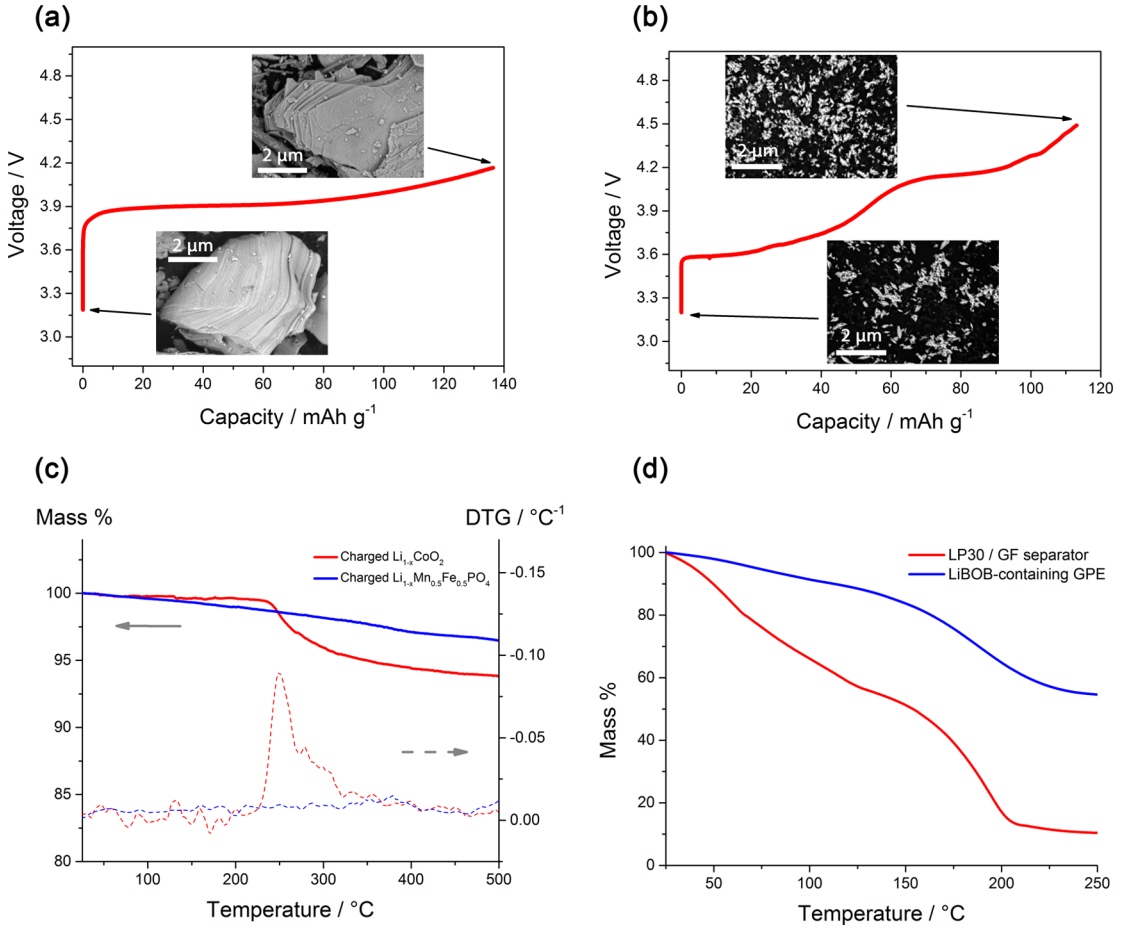

Figure 4. (a) Galvanostatic charge of a $LiCoO_2$ (SC 15, Merck) pellet at 25 °C and 0.2 mA cm^2 in Li/LP30/electrode cell and, in inset, scanning electron micrographs (SEMs) of $LiCoO_2$ and charged $Li_{1-x}CoO_2$. (b) Galvanostatic charge of a $LiMn_{0.5}Fe_{0.5}PO_4$ pellet at 25 °C and 0.2 mA cm^2 in Li/LP30/electrode cell and, in inset, SEMs of $LiMn_{0.5}Fe_{0.5}PO_4$ and charged $(1-x)LiMn_{0.5}Fe_{0.5}PO_4/xMn_{0.5}Fe_{0.5}PO_4$. (c) Thermogravimetric analysis (TGA) of charged $Li_{1-x}CoO_2$ (red) and $(1-x)LiMn_{0.5}Fe_{0.5}PO_4/xMn_{0.5}Fe_{0.5}PO_4$ (blue) performed under a 60 mL min^{-1} N_2 flow at a heating rate of 10 °C min^{-1}. Mass percent on the left *y*-axis (continuous line) and derivative curve (dotted line) on the right *y*-axis. (d) Comparison of thermogravimetric analysis (TGA) of a glass fiber (GF) separator soaked by LP30 (EC:DMC, 1:1, 1 M $LiPF_6$) liquid electrolyte (red) and LiBOB-containing GPE (blue). See Experimental Section for more details.

particular, $LiPF_6$ decomposes above 100 °C in TGA carried out using dry gas flow, according to the following equation[48]

$$LiPF_6 \rightarrow LiF + PF_5 \quad (1)$$

Nevertheless, traces of water significantly reduce the decomposition onset at temperature even lower than 100 °C because of $LiPF_6$ hydrolysis[48]

$$LiPF_6 + H_2O \rightarrow POF_3 + 2HF + LiF \quad (2)$$

In view of these considerations, the small DTG peak observed here at low temperature may be ascribed, according to the eq 2, to reaction with H_2O traces absorbed from atmospheric moisture exposure, just before starting the TGA analysis, while the main DTG peak is likely due to the decomposition according to eq 1. Instead, LiBOB has a remarkable thermal stability, compared to $LiPF_6$, with decomposition starting at about 290 °C (see DTG peak at 338 °C in Figure 3) following the already described[49] reaction:

$$6LiBC_4O_8 \rightarrow 2Li_2C_2O_4 + 2LiB_3O_5 + 10CO + 10CO_2 \quad (3)$$

The further weight loss above 450 °C may be attributed to decomposition of lithium oxalate originated from reaction 3.[49]

Galvanostatic cycling tests at 70 °C have been performed on two $Li/LiMn_{0.5}Fe_{0.5}PO_4$ half-cells using LP30 and 0.7 M LiBOB EC/PC/DMC 1:1:3 w/w liquid electrolytes, in order to compare the high-temperature stability due to the electrolyte salt during cell operation (see Figure 3b–d). Previous studies on LiBOB-alkyl carbonate solutions have shown the poor features of the $LiCoO_2$/electrolyte interface, in particular at the higher temperatures. Jiang et al.[20,50] revealed the limited stability of delithiated $Li_{0.5}CoO_2$ cathode in LiBOB-EC:DEC solutions. In addition, Xu et al.[19] described severe capacity fading upon storage at 60 °C of $Li/LiBOB\text{-}EC{:}DMC/LiCoO_2$ half cells. Instead, the $LiMn_{0.5}Fe_{0.5}PO_4$ olivine cathode studied here is expected to provide higher thermal stability in combination with the LiBOB-EC/PC/DMC electrolyte.

The cycling experiments have been carried out at 1C rate (170 mA g^{-1}). The voltage profiles (Figure 3b) and cycling discharge capacity (Figure 3c) plots show significant increase of the reversible capacity, compared to that observed at room temperature at the same C-rate (compare Figure 3b, c with Figure 1c, d), with values approaching the theoretical one (170 mAh g^{-1}). Such capacity increase is likely ascribed to the enhancement of the lithium diffusion properties of the olivine cathode by thermal activation. The comparison of the voltage

DOI: 10.1021/acsami.5b05179
ACS Appl. Mater. Interfaces 2015, 7, 21198–21207

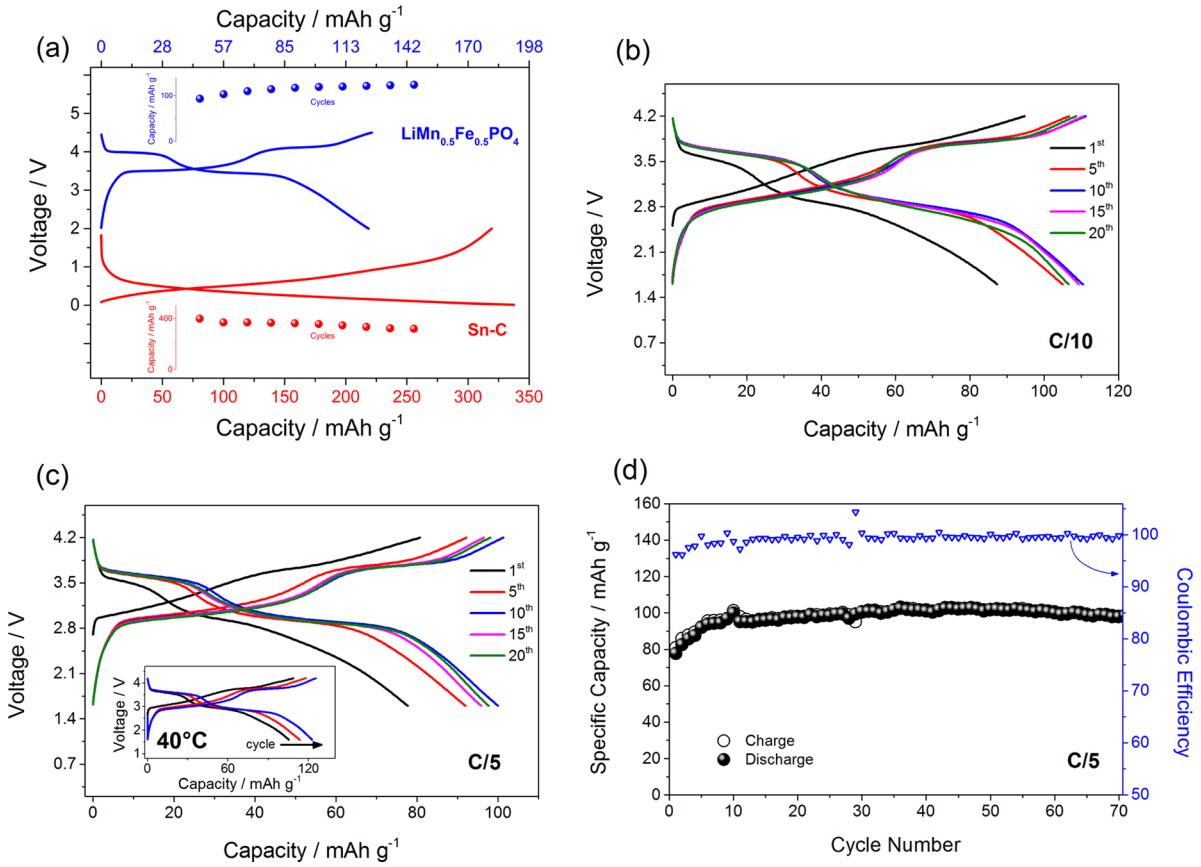

Figure 5. (a) Galvanostatic responses at 25 °C of Li/GPE/$LiMn_{0.5}Fe_{0.5}PO_4$ (in blue) and Li/GPE/Sn−C (in red) half-cells in terms of voltage profiles at steady state condition (10th cycle) and, in inset, in terms of cycling behavior. Li/GPE/$LiMn_{0.5}Fe_{0.5}PO_4$ was tested within the 2−4.5 V voltage range at 0.1C rate (17 mA g^{-1}), whereas Li/GPE/Sn−C cell was tested within the 0.01 V−2 V voltage range at 50 mA g^{-1}. Galvanostatic response at room temperature (25 °C) in terms of voltage profiles of the 1st, 5th, 10th, 15th, and 20th cycle of the Sn−C/GPE/$LiMn_{0.5}Fe_{0.5}PO_4$ full-cell galvanostatically cycled at (b) 0.1C and (c) 0.2C rates (1C = 170 mA $g_{cathode}^{-1}$); inset of panel c: voltage profiles of the 1st, 2nd, and 4th cycle of the full-cell galvanostatically cycled at 40 °C using a 0.2C rate. (d) Cycling behavior at room temperature (25 °C) and corresponding Coulombic efficiency (right *y* axis in blue) of the Sn−C/GPE/$LiMn_{0.5}Fe_{0.5}PO_4$ full-cell galvanostatically cycled at 0.2C rate (1C = 170 mA $g_{cathode}^{-1}$).

profiles of the two cells (Figure 3b) reveals huge irreversible capacity throughout the first cycle for the cell using LP30. During the following cycles the irreversible capacity of the Li/LP30/$LiMn_{0.5}Fe_{0.5}PO_4$ cell significantly decreases, as shown by the Coulombic efficiency plot of Figure 3d. However, Figure 3d reveals higher reversibility for the cell using the LiBOB-containing electrolyte in the whole cycling range, thus suggesting its suitability for full cell application even at the higher temperature levels.

The thermal stability of the $LiMn_{0.5}Fe_{0.5}PO_4$ cathode in its charged state is compared to that of commercial $LiCoO_2$ in Figure 4. Both cathodes have been pressed into pellet and electrochemically delithiated in lithium half-cell at constant current (see Experimental Section for details of the cathode delithiation and recovery procedure). Panels a and b of Figure 4 show the galvanostatic charge profiles of $LiCoO_2$ (a), $LiMn_{0.5}Fe_{0.5}PO_4$ (b), and, in inset, the SEM images of the electrode powders before and after charge. $LiCoO_2$ exhibits the expected voltage profile centered at about 3.9 V upon charge. Considering a charge capacity of about 135 mAh g^{-1} we can estimate that the final lithium content in $Li_{1-x}CoO_2$ is $x \approx 0.5$, which has been indicated as the lithium equivalent limit for reversible Li^+ exchange.[51] The SEM images reveal the typical $LiCoO_2$ layered morphology, which becomes more visible after charge. Meanwhile, the electrochemical delithiation of $LiMn_{0.5}Fe_{0.5}PO_4$ evolves with two expected smooth plateaus at about 3.6 and 4.1 V. The specific charge capacity of $LiMn_{0.5}Fe_{0.5}PO_4$, revealed by Figure 4b (about 115 mAh g^{-1}), suggests that the electrochemical reaction is limited to 0.7 lithium equivalent, i.e., a value indicating a partial conversion of $LiMn_{0.5}Fe_{0.5}PO_4$ to $Mn_{0.5}Fe_{0.5}PO_4$ upon galvanostatic charge. The SEM images show that $LiMn_{0.5}Fe_{0.5}PO_4$ cathode keeps its submicrometrical morphology upon charge without significant modifications.

Figure 4c reports the thermogravimetric behavior of the cathode powders after galvanostatic charge. $Li_{1-x}CoO_2$ ($x \approx 0.5$) shows limited thermal stability, since it starts to decompose at about 240 °C with derivative peak at 250 °C, likely according to the equation[52]

$$Li_{1-x}CoO_2 \rightarrow (1-x)LiCoO_2 + x/3Co_3O_4 + x/3O_2 \quad (4)$$

Instead, the olivine cathode powder after galvanostic charge, having estimated composition $0.3LiMn_{0.5}Fe_{0.5}PO_4/0.7Mn_{0.5}Fe_{0.5}PO_4$, shows a slope due to instrument baseline drift and a thermal stability extended to the whole investigated temperature range without relevant DTG peaks.

Figure 4d shows the TGA curves from RT to 250 °C of the LiBOB-containing GPE and the glass math separator soaked in LP30 electrolyte. The figure reveals that the GPE efficiently mitigates the release of the volatile components upon heating in

DOI: 10.1021/acsami.5b05179
ACS Appl. Mater. Interfaces 2015, 7, 21198−21207

respect to conventional separator soaked by liquid electrolyte, thus suggesting improved safety content of the gel polymer battery. Indeed, both the electrolyte and the cathode material used in the LIB configuration proposed here show higher thermal stability than conventional components.

Figure 5 reports the galvanostatic results of the lithium half-cells formed by coupling the GPE with the $LiMn_{0.5}Fe_{0.5}PO_4$ olivine cathode (Figure 5a, in blue) and the Sn−C nanostructured anode (Figure 5a, in red), as well as the responses at 0.1*C* and 0.2*C* rates (1*C* = 170 mA $g_{cathode}^{-1}$) of the full cell coupling the two electrodes in terms of voltage profile (Figure 5b, c) and cycling behavior (Figure 5d). Figure 5a shows for both half-cells the voltage profiles at the steady state (10th cycle) and, in inset, the discharge and charge capacities throughout cycling of the anode and cathode, respectively. The reported voltage profiles reflect also the cell balance, in terms of positive to negative mass ratio (P/N ratio), whereas the specific capacities (top and down side *x*-axes) are normalized by using the corresponding active material mass loadings. The electrodes mass loading has been carefully tuned by employing an excess of cathode material, in order to allow suitable operation of the full-cell, which is, indeed, limited in respect to the cathode component.

The cathode voltage profile, reported in Figure 5a (blue line), shows two reversible plateaus at about 3.50 and 4.05 V, related to the Fe^{3+}/Fe^{2+} and Mn^{3+}/Mn^{2+} redox couples, respectively, within the olivine structure. This observation is in full agreement with the electrochemical features of the $LiMn_{0.5}Fe_{0.5}PO_4$ material observed in liquid carbonate-based electrolyte (see Figure 1c, d). The Li/GPE/$LiMn_{0.5}Fe_{0.5}PO_4$ cell delivers reversibly a specific capacity of about 120 mAh g^{-1} at 0.1*C* rate (17 mA g^{-1}), i.e., a value of about 70% of the theoretical capacity of the cathode material, in line with the value observed in lithium cell using liquid-electrolyte (see Figures 1c, d, and Figure S1).

A previous electrochemical study of the Sn−C electrode in 0.7 M liquid solution of LiBOB in EC:PC:DMC 1:1:3 (w/w), performed by galvanostatic cycling and supported by voltammetry and electrochemical impedance spectroscopy, evidenced a high-impedance feature of the Sn−C/electrolyte interface. This behavior has been attributed to LiBOB decomposition at about 1.7 V, observed generally for carbonaceous electrodes, during the first cathodic reaction.[22] The same study indicated that partial electrode prelithiation in conventional electrolyte may significantly reduce the interface resistance and remarkably enhance the galvanostatic cell performances in LiBOB-based electrolyte. Therefore, the Sn−C electrode was electrochemically activated in lithium cell using LP30 electrolyte prior to assemble the Li/GPE/Sn−C cell (see the Experimental Section for details of the procedure). Figure 5a (red curves), reporting the cycling behavior of the Li/GPE/Sn−C half-cell, shows a working voltage of about 0.5 V, ascribed to the lithium−tin alloying/dealloying process, and a stable specific capacity of about 350 mAh g^{-1}, approaching 78% of the theoretical value of the Sn−C electrode (450 mAh g^{-1}).[38,41]

Panels b, c, and d of Figure 5 report the galvanostatic cycling response of the Sn−C/GPE/$LiMn_{0.5}Fe_{0.5}PO_4$ full Li-ion cell at room temperature. Figure 5(b, c) shows the voltage profiles at 0.1*C* and 0.2*C* rates, respectively, and Figure 5d the cycling behavior at 0.2*C* rate upon 70 cycles (1*C* = 170 mA $g_{cathode}^{-1}$). In addition, inset of Figure 5c shows the response of the cell cycled at 40 °C at 0.2*C* rate. The full-cell reveals a signature arising from lithium insertion/deinsertion reaction within the $LiMn_{0.5}Fe_{0.5}PO_4$ lattice at the cathode side and Li−Sn−C alloying/dealloying process at the anode side, according to the following equation:

$$Sn - C + xLiMn_{0.5}Fe_{0.5}PO_4 \leftrightarrow Li_xSn - C + xMn_{0.5}Fe_{0.5}PO_4 \quad (5)$$

with $x < 4.4$. The increasing capacity trend observed during the initial cycles in Figure 5 is most likely due to the already observed structural reorganizations of olivine structure (see Figure 1c, d).

The galvanostatic response of the Sn−C/GPE/$LiMn_{0.5}Fe_{0.5}PO_4$ is comparable to that observed in analogous liquid configuration with standard LP30 electrolyte (see Figure S2). At steady state, the cell delivers reversible capacities of about 110 mAh g^{-1} and 100 mAh g^{-1} at 0.1*C* and 0.2*C* rates, respectively, through two discharge voltage plateaus at about 2.8 and 3.6 V. Accordingly, the estimated theoretical energy density referred to the cathode is about 360 Wh kg^{-1}. At higher temperature the cell shows increased discharge capacity likely due to thermal activation of the olivine cathode as well as the GPE (see inset of Figure 5b). The full cell cycled at room temperature at 0.2*C* rate shows stable behavior for 70 cycles with a Coulombic efficiency approaching 100%.

CONCLUSION

In this paper, we investigated the electrochemical properties of a gel polymer electrolyte (GPE) formed by entrapping a LiBOB salt within a PVdF-EC-PC-DMC polymer matrix. Our results revealed an ionic conductivity of the order of 1×10^{-3} S cm^{-1} with a wide electrochemical stability window, extending up to 4.9 V. The electrolyte evidenced moderate stability of the Li/GPE interface, in particular upon long-term cycling, thus suggesting the replacement of the lithium metal by alternative anode as suitable strategy for efficient cell application. We employed the GPE in a full Sn−C/$LiMn_{0.5}Fe_{0.5}PO_4$ lithium-ion battery.

The $LiMn_{0.5}Fe_{0.5}PO_4$ olivine cathode was synthesized by solvothermal method. In particular, our results confirmed the formation of a $LiMn_{1-x}Fe_xPO_4$ solid solution, with no evidence of segregation of $LiMnPO_4$ and $LiFePO_4$ phases within the olivine structure. Thermogravimetric measurements confirmed the higher intrinsic stability of both LiBOB and delithiated $Mn_{0.5}Fe_{0.5}PO_4$ cathode when compared to that of conventional $LiPF_6$ and $Li_{0.5}CoO_2$, and revealed decreased volatile components release upon heating for the GPE configuration.

The GPE was studied in Li/GPE/Sn−C and Li/GPE/$LiMn_{0.5}Fe_{0.5}PO_4$ half-cells by galvanostatic cycling. Following the electrode evaluation in half-cells, we characterized the lithium-ion cell formed by coupling nanostructured Sn−C anode and olivine $LiMn_{0.5}Fe_{0.5}PO_4$ cathode within the proposed gel configuration. The full-cell revealed a reversible capacity of about 110 mAh g^{-1}, with two working voltages at about 2.8 and 3.6 V, a Coulombic efficiency of about 99%, and an estimated theoretical energy density of about 360 Wh kg^{-1} with respect to the cathode . The battery is expected to allow a practical energy density value comparable to that of the commercial LIBs,[53] as well as an intrinsic high safety content due to the use of fluorine-free lithium salt, the gelled configuration, and the employment of an olivine cathode characterized by a stable polyanionic framework. External short circuit and nail penetration tests may be suitable to fully verify the safety content of our cell. These tests, projected for large scale systems rather than laboratory prototypes, may require a

DOI: 10.1021/acsami.5b05179
ACS Appl. Mater. Interfaces 2015, 7, 21198−21207

scaling up to battery size benefiting of proper cell case and geometry. This will be certainly an ambitious target, which may be achieved by the support of specialized laboratories.

■ ASSOCIATED CONTENT

Supporting Information

The Supporting Information is available free of charge on the ACS Publications website at DOI: 10.1021/acsami.5b05179.

Galvanostatic cycling response of the $LiMn_{0.5}Fe_{0.5}PO_4$ cathode used as the working electrode in lithium half-cell with standard LP30 electrolyte; galvanostatic cycling response of a full Sn−C/LP30/$LiMn_{0.5}Fe_{0.5}PO_4$ lithium-ion cell (PDF)

■ AUTHOR INFORMATION

Corresponding Author

*E-mail: jusef.hassoun@unife.it.

Notes

The authors declare no competing financial interest.

■ REFERENCES

(1) Balakrishnan, P. G.; Ramesh, R.; Prem Kumar, T. Safety Mechanisms in Lithium-Ion Batteries. *J. Power Sources* **2006**, *155*, 401−414.

(2) Xu, K. Nonaqueous Liquid Electrolytes for Lithium-Based Rechargeable Batteries. *Chem. Rev.* **2004**, *104*, 4303−4417.

(3) Gnanaraj, J. S.; Zinigrad, E.; Asraf, L.; Gottlieb, H. E.; Sprecher, M.; Schmidt, M.; Geissler, W.; Aurbach, D. A Detailed Investigation of the Thermal Reactions of $LiPF_6$ Solution in Organic Carbonates Using ARC and DSC. *J. Electrochem. Soc.* **2003**, *150*, A1533−A1537.

(4) Aurbach, D.; Markovsky, B.; Salitra, G.; Markevich, E.; Talyossef, Y.; Koltypin, M.; Nazar, L.; Ellis, B.; Kovacheva, D. Review on Electrode-Electrolyte Solution Interactions, Related to Cathode Materials for Li-Ion Batteries. *J. Power Sources* **2007**, *165*, 491−499.

(5) Aravindan, V.; Gnanaraj, J.; Madhavi, S.; Liu, H. K. Lithium-Ion Conducting Electrolyte Salts for Lithium Batteries. *Chem. - Eur. J.* **2011**, *17*, 14326−14346.

(6) Choi, N. S.; Chen, Z.; Freunberger, S. a.; Ji, X.; Sun, Y. K.; Amine, K.; Yushin, G.; Nazar, L. F.; Cho, J.; Bruce, P. G. Challenges Facing Lithium Batteries and Electrical Double-Layer Capacitors. *Angew. Chem., Int. Ed.* **2012**, *51*, 9994−10024.

(7) Manuel Stephan, A. Review on Gel Polymer Electrolytes for Lithium Batteries. *Eur. Polym. J.* **2006**, *42*, 21−42.

(8) Hassoun, J.; Reale, P.; Scrosati, B. Recent Advances in Liquid and Polymer Lithium-Ion Batteries. *J. Mater. Chem.* **2007**, *17*, 3668−3677.

(9) Xu, K. Electrolytes and Interphases in Li-Ion Batteries and Beyond. *Chem. Rev.* **2014**, *114*, 11503−11618.

(10) Zhang, S. S. A Review on Electrolyte Additives for Lithium-Ion Batteries. *J. Power Sources* **2006**, *162*, 1379−1394.

(11) Xu, K.; Zhang, S.; Jow, T. R.; Xu, W.; Angell, C. A. LiBOB as Salt for Lithium-Ion Batteries: A Possible Solution for High Temperature Operation. *Electrochem. Solid-State Lett.* **2002**, *5*, A26−A29.

(12) Xu, W.; Angell, C. a. LiBOB and Its Derivatives: Weakly Coordinating Anions, and the Exceptional Conductivity of Their Nonaqueous Solutions. *Electrochem. Solid-State Lett.* **2001**, *4*, E1−E7.

(13) Jiang, J.; Dahn, J. R. Effects of Solvents and Salts on the Thermal Stability of LiC_6. *Electrochim. Acta* **2004**, *49*, 4599−4604.

(14) Liu, Z.; Chai, J.; Xu, G.; Wang, Q.; Cui, G. Functional Lithium Borate Salts and Their Potential Application in High Performance Lithium Batteries. *Coord. Chem. Rev.* **2015**, *292*, 56−73.

(15) Larush-Asraf, L.; Biton, M.; Teller, H.; Zinigrad, E.; Aurbach, D. On the Electrochemical and Thermal Behavior of Lithium Bis-(oxalato)borate (LiBOB) Solutions. *J. Power Sources* **2007**, *174*, 400−407.

(16) Xu, K.; Zhang, S.; Poese, B. a.; Jow, T. R. Lithium Bis(oxalato)borate Stabilizes Graphite Anode in Propylene Carbonate. *Electrochem. Solid-State Lett.* **2002**, *5*, A259−A262.

(17) Jiang, J.; Dahn, J. R. Comparison of the Thermal Stability of Lithiated Graphite in LiBOB EC/DEC and in $LiPF_6$ EC/DEC. *Electrochem. Solid-State Lett.* **2003**, *6*, A180−A182.

(18) Chen, Z.; Lu, W. Q.; Liu, J.; Amine, K. $LiPF_6$/LiBOB Blend Salt Electrolyte for High-Power Lithium-Ion Batteries. *Electrochim. Acta* **2006**, *51*, 3322−3326.

(19) Xu, K.; Zhang, S. S.; Lee, U.; Allen, J. L.; Jow, T. R. LiBOB: Is it an Alternative Salt for Lithium Ion Chemistry? *J. Power Sources* **2005**, *146*, 79−85.

(20) Jiang, J.; Dahn, J. R. ARC Studies of the Thermal Stability of Three Different Cathode Materials: $LiCoO_2$; $Li[Ni_{0.1}Co_{0.8}Mn_{0.1}]O_2$; and $LiFePO_4$, in $LiPF_6$ and LiBOB EC/DEC electrolytes. *Electrochem. Commun.* **2004**, *6*, 39−43.

(21) Amine, K.; Liu, J.; Kang, S.; Belharouak, I.; Hyung, Y.; Vissers, D.; Henriksen, G. Improved Lithium Manganese Oxide Spinel/Graphite Li-Ion Cells for High-Power Applications. *J. Power Sources* **2004**, *129*, 14−19.

(22) Hassoun, J.; Wachtler, M.; Wohlfahrt-Mehrens, M.; Scrosati, B. Electrochemical Behaviour of Sn and Sn-C Composite Electrodes in LiBOB Containing Electrolytes. *J. Power Sources* **2011**, *196*, 349−354.

(23) Aravindan, V.; Lee, Y.-S.; Madhavi, S. Research Progress on Negative Electrodes for Practical Li-Ion Batteries: Beyond Carbonaceous Anodes. *Adv. Energy Mater.* **2015**, *5*, 1402225.

(24) Aravindan, V.; Gnanaraj, J.; Lee, Y.-S.; Madhavi, S. $LiMnPO_4$ − A Next Generation Cathode Material for Lithium-Ion Batteries. *J. Mater. Chem. A* **2013**, *1*, 3518−3539.

(25) Saravanan, K.; Ramar, V.; Balaya, P.; Vittal, J. J. $Li(Mn_xFe_{1-x})PO_4/C$ (x = 0.5, 0.75 and 1) Nanoplates for Lithium Storage Application. *J. Mater. Chem.* **2011**, *21*, 14925−14935.

(26) Baek, D. H.; Kim, J. K.; Shin, Y. J.; Chauhan, G. S.; Ahn, J. H.; Kim, K. W. Effect of Firing Temperature on the Electrochemical Performance of $LiMn_{0.4}Fe_{0.6}PO_4/C$ Materials Prepared by Mechanical Activation. *J. Power Sources* **2009**, *189*, 59−65.

(27) Yamada, A.; Chung, S.-C. Crystal Chemistry of the Olivine-Type $Li(Mn_yFe_{1-y})PO_4$ and $(Mn_yFe_{1-y})PO_4$ as Possible 4 V Cathode Materials for Lithium Batteries. *J. Electrochem. Soc.* **2001**, *148*, A960−A967.

(28) Kobayashi, G.; Yamada, A.; Nishimura, S. I.; Kanno, R.; Kobayashi, Y.; Seki, S.; Ohno, Y.; Miyashiro, H. Shift of Redox Potential and Kinetics in $Li_x(Mn_yFe_{1-y})PO_4$. *J. Power Sources* **2009**, *189*, 397−401.

(29) Oh, S.-M.; Myung, S.-T.; Choi, Y. S.; Oh, K. H.; Sun, Y.-K. Co-Precipitation Synthesis of Micro-Sized Spherical $LiMn_{0.5}Fe_{0.5}PO_4$ Cathode Material for Lithium Batteries. *J. Mater. Chem.* **2011**, *21*, 19368−19374.

(30) Chen, L.; Yuan, Y.-Q.; Feng, X.; Li, M.-W. Enhanced Electrochemical Properties of $LiFe_{1-x}Mn_xPO_4/C$ Composites Synthesized from $FePO_4{\cdot}2H_2O$ Nanocrystallites. *J. Power Sources* **2012**, *214*, 344−350.

(31) Zhang, B.; Wang, X.; Li, H.; Huang, X. Electrochemical Performances of $LiFe_{1-x}Mn_xPO_4$ with High Mn Content. *J. Power Sources* **2011**, *196*, 6992−6996.

(32) Damen, L.; De Giorgio, F.; Monaco, S.; Veronesi, F.; Mastragostino, M. Synthesis and Characterization of Carbon-Coated $LiMnPO_4$ and $LiMn_{1-x}Fe_xPO_4$ (x = 0.2, 0.3) Materials for Lithium-Ion Batteries. *J. Power Sources* **2012**, *218*, 250−253.

(33) Jo, M.; Yoo, H.; Jung, Y. S.; Cho, J. Carbon-Coated Nanoclustered $LiMn_{0.71}Fe_{0.29}PO_4$ Cathode for Lithium-Ion Batteries. *J. Power Sources* **2012**, *216*, 162−168.

(34) Oh, S.-M.; Myung, S.-T.; Park, J. B.; Scrosati, B.; Amine, K.; Sun, Y.-K. Double-Structured $LiMn_{(0.85)}Fe_{(0.15)}PO_4$ Coordinated with $LiFePO_4$ for Rechargeable Lithium Batteries. *Angew. Chem., Int. Ed.* **2012**, *51*, 1853−1856.

(35) Zhong, Y. J.; Li, J. T.; Wu, Z. G.; Guo, X. D.; Zhong, B. H.; Sun, S. G. $LiMn_{0.5}Fe_{0.5}PO_4$ Solid Solution Materials Synthesized by Rheological Phase Reaction and Their Excellent Electrochemical

DOI: 10.1021/acsami.5b05179
ACS Appl. Mater. Interfaces 2015, 7, 21198−21207

Performances as Cathode of Lithium Ion Battery. *J. Power Sources* **2013**, *234*, 217−222.
(36) Hong, Y.; Tang, Z.; Hong, Z.; Zhang, Z. $LiMn_{1-x}Fe_xPO_4$ (x = 0, 0.1, 0.2) Nanorods Synthesized by a Facile Solvothermal Approach as High Performance Cathode Materials for Lithium-Ion Batteries. *J. Power Sources* **2014**, *248*, 655−659.
(37) Hu, L.; Qiu, B.; Xia, Y.; Qin, Z.; Qin, L.; Zhou, X.; Liu, Z. Solvothermal Synthesis of Fe-Doping $LiMnPO_4$ Nanomaterials for Li-Ion Batteries. *J. Power Sources* **2014**, *248*, 246−252.
(38) Hassoun, J.; Derrien, G.; Panero, S.; Scrosati, B. A Nanostructured Sn-C Composite Lithium Battery Electrode with Unique Stability and High Electrochemical Performance. *Adv. Mater.* **2008**, *20*, 3169−3175.
(39) Brutti, S.; Manzi, J.; De Bonis, a.; Di Lecce, D.; Vitucci, F.; Paolone, a.; Trequattrini, F.; Panero, S. Controlled Synthesis of $LiCoPO_4$ by a Solvo-Thermal Method at 220°C. *Mater. Lett.* **2015**, *145*, 324−327.
(40) Fasciani, C.; Panero, S.; Hassoun, J.; Scrosati, B. Novel Configuration of Poly(vinylidenedifl uoride)-Based Gel Polymer Electrolyte for Application in Lithium-Ion Batteries. *J. Power Sources* **2015**, *294*, 180−186.
(41) Hassoun, J.; Lee, K.-S.; Sun, Y.-K.; Scrosati, B. An Advanced Lithium Ion Battery Based on High Performance Electrode Materials. *J. Am. Chem. Soc.* **2011**, *133*, 3139−3143.
(42) Padhi, A. K.; Nanjundaswamy, K. S.; Goodenough, J. B. Phospho-olivines as Positive-Electrode Materials for Rechargeable Lithium Batteries. *J. Electrochem. Soc.* **1997**, *144*, 1188−1194.
(43) Hu, P.; Duan, Y.; Hu, D.; Qin, B.; Zhang, J.; Wang, Q.; Liu, Z.; Cui, G.; Chen, L. Rigid−Flexible Coupling High Ionic Conductivity Polymer Electrolyte for an Enhanced Performance of $LiMn_2O_4$/Graphite Battery at Elevated Temperature. *ACS Appl. Mater. Interfaces* **2015**, *7*, 4720−4727.
(44) Zhang, J.; Yue, L.; Hu, P.; Liu, Z.; Qin, B.; Zhang, B.; Wang, Q.; Ding, G.; Zhang, C.; Zhou, X.; Yao, J.; Cui, G.; Chen, L. Taichi-Inspired Rigid-Flexible Coupling Cellulose-Supported Solid Polymer Electrolyte for High-Performance Lithium Batteries. *Sci. Rep.* **2014**, *4*, 6272.
(45) Panitz, J. C.; Wietelmann, U.; Wachtler, M.; Ströbele, S.; Wohlfahrt-Mehrens, M. Film Formation in LiBOB-Containing Electrolytes. *J. Power Sources* **2006**, *153*, 396−401.
(46) Li, S.; Ma, P.; Cui, X.; Ren, Q.; Li, F. Studies on the Thermal Decomposition Kinetics of $LiPF_6$ and $LiBC_4O_8$. *Proc. - Indian Acad. Sci., Chem. Sci.* **2008**, *120*, 289−292.
(47) Lekgoathi, M. D. S.; Vilakazi, B. M.; Wagener, J. B.; Le Roux, J. P.; Moolman, D. Decomposition Kinetics of Anhydrous and Moisture Exposed $LiPF_6$ Salts by Thermogravimetry. *J. Fluorine Chem.* **2013**, *149*, 53−56.
(48) Yang, H.; Zhuang, G. V.; Ross, P. N. Thermal Stability of $LiPF_6$ Salt and Li-Ion Battery Electrolytes Containing $LiPF_6$. *J. Power Sources* **2006**, *161*, 573−579.
(49) Zinigrad, E.; Larush-Asraf, L.; Salitra, G.; Sprecher, M.; Aurbach, D. On the Thermal Behavior of Li Bis(oxalato)borate LiBOB. *Thermochim. Acta* **2007**, *457*, 64−69.
(50) Jiang, J.; Dahn, J. R. Effects of Particle Size and Electrolyte Salt on the Thermal Stability of $Li_{0.5}CoO_2$. *Electrochim. Acta* **2004**, *49*, 2661−2666.
(51) Croguennec, L.; Palacin, M. R. Recent Achievements on Inorganic Electrode Materials for Lithium Ion Batteries. *J. Am. Chem. Soc.* **2015**, *137*, 3140−3156.
(52) Dahn, J.; Fuller, E.; Obrovac, M.; Vonsacken, U. Thermal Stability of Li_xCoO_2, Li_xNiO_2 and λ-MnO_2 and consequences for the Safety of Li-ion Cells. *Solid State Ionics* **1994**, *69*, 265−270.
(53) Thackeray, M. M.; Wolverton, C.; Isaacs, E. D. Electrical Energy Storage for Transportation—Approaching the Limits of, and Going Beyond, Lithium-Ion Batteries. *Energy Environ. Sci.* **2012**, *5*, 7854−7863.

DOI: 10.1021/acsami.5b05179
ACS Appl. Mater. Interfaces 2015, 7, 21198−21207